



HAL
open science

New injectable self-assembled hydrogels that promote angiogenesis through a bioactive degradation product

K.R. Sindhu, N. Bansode, M. Rémy, C. Morel, R. Bareille, M. Hagedorn, B. Hinz, P. Barthélémy, O. Chassande, C. Boiziau

► To cite this version:

K.R. Sindhu, N. Bansode, M. Rémy, C. Morel, R. Bareille, et al.. New injectable self-assembled hydrogels that promote angiogenesis through a bioactive degradation product. *Acta Biomaterialia*, 2020, 115, pp.197-209. 10.1016/j.actbio.2020.08.012 . hal-03413386

HAL Id: hal-03413386

<https://hal.science/hal-03413386>

Submitted on 26 Sep 2022

HAL is a multi-disciplinary open access archive for the deposit and dissemination of scientific research documents, whether they are published or not. The documents may come from teaching and research institutions in France or abroad, or from public or private research centers.

L'archive ouverte pluridisciplinaire **HAL**, est destinée au dépôt et à la diffusion de documents scientifiques de niveau recherche, publiés ou non, émanant des établissements d'enseignement et de recherche français ou étrangers, des laboratoires publics ou privés.



Distributed under a Creative Commons Attribution - NonCommercial 4.0 International License

New injectable self-assembled hydrogels that promote angiogenesis through a bioactive degradation product

Sindhu, K.R.^{1,2,\$}, Bansode, N.^{3,4,\$}, Rémy, M.¹, Morel, C.¹, Bareille, R.¹, Hagedorn, M.⁵, Hinz, B.⁶, Barthélémy, P.³, Chassande, O.¹ & Boiziau, C.^{1,*}

1: INSERM, Univ. Bordeaux, BIOTIS, F-33000 Bordeaux, France.

2: Present address: INSERM, Univ. Lille, U1008-Controlled Drug Delivery Systems and Biomaterials, F-59000 Lille, France

3: INSERM, Univ. Bordeaux, ARNA Laboratory, F-33000 Bordeaux, France.

4: Present address: CNRS, Univ. Bordeaux, ENSCBP, Laboratoire de Chimie des Polymeres Organiques (LCPO), UMR 5629, F-33607 Pessac cedex, France

5: INSERM, Univ. Bordeaux, Biotherapy of Genetic Diseases, Inflammatory Disorders and Cancers, F-33000 Bordeaux, France.

6: Laboratory of Tissue Repair and Regeneration, Faculty of Dentistry, University of Toronto, Toronto, Ontario, Canada.

\$ Equal contribution.

* **To whom correspondence should be addressed: claudine.boiziau@inserm.fr.** Inserm U1026, University of Bordeaux, 146, rue Leo Saignat, F-33 076 Bordeaux cedex, France.

ABSTRACT

Hydrogels used in regenerative medicine are often designed to allow cellular infiltration, degradation, and neovascularization. Low molecular weight hydrogels (LMWHs), formed by self-assembly *via* non-covalent interactions, are gaining significant interest because they are soft, easy to use and injectable. We propose LMWHs as suitable body implant materials that can stimulate tissue regeneration. We produced four new LMWHs with molecular entities containing nucleic acid and lipid building blocks and analyzed the foreign body response upon subcutaneous implantation into mice. Despite being infiltrated with macrophages, none of the hydrogels triggered detrimental inflammatory responses. Most macrophages present in the hydrogel-surrounding tissue acquired an immuno-modulatory rather than inflammatory phenotype. Concomitantly, no fibrotic capsule was formed after three weeks. Our **glyconucleolipid** LMWHs exhibited different degradation kinetics *in vivo* and *in vitro*. LMWHs with high angiogenic properties *in vivo*, were found to release glyconucleoside (glucose covalently linked to thymidine *via* a triazole moiety) as a common by-product of *in vitro* LMWH degradation. Chemically synthesized glyconucleoside exhibited angiogenic properties *in vitro* in scratch assays with monolayers of human endothelial cells and *in vivo* using the chick chorioallantoic membrane assay. Collectively, LMWHs hold promise as efficient scaffolds for various regenerative applications by displaying good biointegration without causing fibrosis, and by promoting angiogenesis through the release of a pro-angiogenic degradation product.

Key words: hydrogel; biointegration; fibrosis; angiogenesis; tissue regeneration.

1. INTRODUCTION

The worldwide aging population and unhealthy lifestyles increase the need for durable and efficient medical devices that support failing tissue or maintain homeostasis of biological processes. Various biomaterials are used in different medical applications such as scaffolds for regeneration of defective tissues, drug delivery, or coating implantable medical devices. To increase the success of regenerative medicine applications, biomaterials are developed as alternatives to organ transplantation, to be used either alone or in combination with cells and/or biomolecules [1–3].

All materials that are injected or implanted in the body are facing the same fundamental challenges: i) they must be biocompatible with low if any cytotoxicity of the initial structure and possible degradation products; ii) inflammatory reactions to biomaterials must be managed to prevent degradation of the biomaterial before successful tissue regeneration is reached, and to avoid exacerbated and/or chronic inflammation; iii) foreign body reaction (FBR), which is a physiological tissue repair response **and most often results in the development of a fibrous capsule** [4–8], must be minimized. Indeed, this fibrotic capsule impedes diffusion of nutrients and metabolites, often leading to failure of the medical device. To date, several attempts have been made to develop biomaterials that reduce the capsule formation, albeit with limited success.

Hydrogels meet most of the requirements of successful biomaterials and are gaining traction as scaffolds used in successful regenerative medicine applications. All hydrogels are hydrophilic, which facilitates diffusion of oxygen and nutrients and, in some cases, supports cell colonization. Hydrogels are easy to use, often injectable, and have tunable mechanical properties [9]. Local swelling and gelling allow adaptation of hydrogel materials to the 3D structure of the local host environment. Among self-assembled physical hydrogels, low molecular weight hydrogels (LMWHs), which are made of small amphiphilic molecules, are receiving increasing attention. LMWHs are formed through reversible non-covalent interactions such as hydrogen bonding, π - π stacking, hydrophobic effects, and ion pairing. Recently, LMWHs composed of synthetic hybrid molecules, combining biomolecules such as nucleic acid and lipids, have been investigated as low molecular weight hydrogelators [10]. Upon cooling below the temperature of gelation, these molecules self-assemble into a three-dimensional (3D) entangled network of solid

fibers, immobilizing the liquid phase through strong intermolecular forces [11]. The advantage of such a process is that no crosslinking agent is required for gel formation, such as reactive chemicals, UV light, or drastic change in pH, which may be toxic for cells or tissues. Glyconucleolipids represent a subfamily of LMWHs that spontaneously form hydrogels at mammalian body temperatures. Gel formation kinetics, ultrastructure, and mechanical properties can be controlled through the chemical structure of the building block compound. However, the relationship between chemical composition and physical properties of the resulting gels is incompletely understood and must be experimentally determined for every new compound [12–14].

To produce biomaterials **combining injectability, the best possible capacity for biointegration (reduced inflammation and fibrosis), and that display various degradation rates to fit the requirements of either a tissue engineering support or a drug delivery system**, we chose four glyconucleolipid LMWHs with previously characterized physical properties (**Fig. 1**): i) three glyconucleoside bolaamphiphiles (GNBA) featuring the hydrophobic moiety functionalized with urea or amide and N-thymine glycosylated head groups conjugated *via* aromatic triazoline ring and ii) a glycosyl-nucleosyl-fluorinated (GNF) compound first synthesized in 2010 [15–19]. GNBA and GNF compounds bear similar structures (single chain amphiphile *versus* bolaamphiphiles) with different functional groups (urea, amide). The LMWHs GNBA-1 and GNBA-2 contain urea functionality next to the aromatic functionality (**Fig. 1, gray box**) which enhances π - π interactions and hydrophobic interactions through two hydrogen bonds in ureido group. Conversely, the LMWHs GNF and GNBA-3 containing amide functionality (**Fig. 1, gray box**) are only weakly associated due to only one hydrogen bond which leads to lower π - π interactions and hydrophobic interactions. GNBA-1 and -2 were selected because they exhibit slightly different gelling kinetics although they only differ by one CH_2 moiety. Indeed, GNF, GNBA-1, GNBA-2 and GNBA-3 were shown to form gels within 23 minutes, 40 seconds, 44 minutes and 3 minutes, respectively. Their respective elastic moduli (G') were 1.7 kPa, 11 kPa, 12 kPa and 5 kPa. In previous publications, we showed that the

supramolecular properties of nucleolipids and glyconucleolipids allow sustained drug release [20], use in tissue engineering [21], and use as bioinspired materials [22].

This study was designed in order to compare the biological properties of these gels, with two goals: i) to establish the relationship between chemical formula, gelation characteristics, rheological properties, *in vitro* degradation rate, and protein adsorption on the one hand and *in vivo* behavior such as stability, inflammatory response, and angiogenesis on the other hand; ii) identify the potential therapeutic applications of these compounds, based on their *in vitro* and *in vivo* behaviors. We show that our **glyconucleolipid** LMWHs are injectable and upon subcutaneous injection, degrade with various kinetics without inducing exacerbated inflammation and the formation of a fibrous capsule. We found that upon degradation, three out of four hydrogels release a by-product with pro-angiogenic properties. Thus, in medical applications such as tissue engineering, where angiogenesis is a success parameter, these three hydrogels are promising scaffolds.

2. MATERIALS AND METHODS

2.1. Hydrogel preparation

The following molecules were used to prepare the hydrogels at a concentration of 1.5 % (w/v) in sterile phosphate-buffered saline (PBS) at pH 7.4: GNF [23] and three GNBA (GNBA-1, GNBA-2, and GNBA-3), corresponding to products 16, 18, and 12 in Ramin *et al* [24]. Suspensions were heated at 65°C for GNF and 80°C for the three GNBA. The GNF solution was incubated at 37°C for 30 min to form a gel, whereas the other molecules formed the gel within 5 min at room temperature.

2.2. *In vitro* degradation of hydrogels and analysis of degradation products

To assess *in vitro* degradation/disassembly over time, hydrogel disks (100 µL) were incubated in 7 mL of PBS at 37°C for 21 d and weighed at different time points; all hydrogel samples were pre-weighed after gelation. At different times (1, 2, 3, 5, 7, 15, and 21 d), the samples were removed from PBS, weighed immediately after removing the excess of PBS by gently wiping the surface with Kimwipes, and returned to the PBS solution. Results are expressed as a percentage of weight loss over time (done in triplicates). The degradation products generated during the 21 d incubation of the samples were identified by submitting the PBS solution in which LMWHs were incubated (see section 2.2) to mass spectrometry analysis. One of the degradation products common to GNF, GNBA-1 and GNBA-3, a glyconucleoside called GN-1, which was supposed to have angiogenic properties (see below section 3.5), was chemically synthesized (Suppl. S1).

2.3. *In vitro* protein adsorption on hydrogels

To investigate non-specific protein adsorption, the adsorption of bovine serum albumin (BSA, GE-healthcare ref K45-001) was evaluated. Hydrogels were cut into pieces with a diameter of 4.7 mm and a height of 5.7 mm (volume of 100 µL, the surface of 120 mm²) followed by incubation in PBS overnight at 37°C to reach the swelling equilibrium. On the following day, the PBS was replaced by 400 µL PBS containing BSA (2 mg/mL, freshly prepared), followed by incubation in a 48 well plate at 37°C for 2 h. Samples were then rinsed thoroughly several times with PBS to remove unbound BSA, followed by addition of 400 µL of

sodium dodecyl sulfate solution 1 % (w/v, Sigma-Aldrich, France) per well for 30 min at room temperature to strip proteins adsorbed on the hydrogel surface. The **stripped** BSA protein was quantified using a standard bicinchoninic acid protein assay (BCA, Pierce™ BCA Protein Assay Kit) as recommended by the manufacturer. The negative control was performed in a similar way excluding the incubation step with BSA. Experiments were performed in triplicates.

2.4. Cytotoxicity assessment

Cytotoxicity of hydrogels was assessed according to the international standard ISO10993-5 (Biological evaluation of medical devices - Part 5: Tests for *in vitro* cytotoxicity). **Hydrogel extracts were prepared by incubation of hydrogel pieces (diameter 4.7 mm, height 5.7 mm) in the culture medium (alpha-MEM (Gibco, Ref A10490-01, France) without ascorbic acid) at 37°C for 24 h, providing the “24(1)” extract (ratio between the surface area of the sample and the volume of the vehicle: 5 cm²/mL). New medium was added on LMWH pieces for a second and then a third incubation of 24 h at 37°C, providing “24(2)” and “24(3)” extracts. At the end, all extracts were stored at -80°C, and supplemented with 10% (v/v) foetal calf serum (FCS, Lonza, France) before being used with the test cell line.**

The L929 cell line (recommended by the standard) **was** grown in alpha-MEM containing 10 % (v/v) FCS. Cells were then seeded at 10,000 cells/cm² in 24 well microtiter plates (Nunc, Denmark) and cultured for 72 h. At subconfluency (3 d culture), **1 mL of the extracts was added on the cells**. Wells containing only alpha-MEM + 10% FCS were used as negative controls, wells with 0.1% Triton X100 were used as a positive control (“Toxic control”). Culture plates were then kept in the incubator at 37°C for 24 h. At the end of this incubation, cell viability was assessed by the Neutral Red assay and cell metabolic activity by using an MTT assay. MTT (3-(4, 5-dimethylthiazolyl-2)-2, 5-diphenyltetrazolium bromide, Sigma-Aldrich, ref M2128) (1 mg/mL stock in alpha-MEM without FCS without phenol red) was added in 125 µL per well. After 3 h of incubation at 37°C in 5% CO₂, the supernatant was removed and formed formazan crystals were dissolved by adding 100 µL of dimethyl sulfoxide (DMSO, Ref D5879-1L, Sigma-Aldrich, France). Neutral red (Ref N4638, Sigma-Aldrich, France) was dissolved at 1.25% (w/v) in alpha-MEM without FCS, and 100 µL of the prepared solution was added per well. After 3 h of incubation at 37°C, the supernatant was replaced by 100 µL of a mixture (50:50) containing 50% ethanol/ 1% acetic acid in water to lyse the cells. In both cases, color intensity was

quantified by measuring the absorbance at 540 nm using a spectrophotometer (Perkin Elmer®, 2030 Multilabel Reader VictorTMX3). The mean values of absorbance measurements obtained from colorimetric tests and their corresponding standard deviation (\pm s.d.) were calculated from 5 repeats. The results are expressed as a percentage of the negative control (alpha-MEM + 10% FCS).

In addition, direct contact cytotoxicity was assessed by placing pieces of LMWHs in inserts immersed in the culture medium (alpha-MEM containing 10% FCS) using Falcon inserts (Ref: 353096, 24 well format). The ratio of the sample surface area to the volume of the vehicle was 5 cm²/mL. Primary cell culture of human adipose tissue-derived mesenchymal stromal cells (MSCs) was performed in parallel with the L929 cell line for 3 d before being in contact with the LMWHs in inserts. After addition of inserts, culture plates were kept in the incubator at 37°C for 24 h providing the “24(1)” cell culture; then, the inserts were transferred on other sub-confluent L929 and MSC cultures for a second and then a third incubation of 24 h, providing “24(2)” and “24(3)” cell cultures. At the end of each 24 h incubation, cell viability was assessed by the Neutral Red assay and cell metabolic activity by using an MTT assay, as described above.

2.5. Migration and proliferation of human umbilical vein endothelial cells (HUVEC).

Based on the supposed pro-angiogenic properties of the glyconucleoside GN-1 released during GNF, GNBA-1 and GNBA-3 *in vitro* degradation, the effects of this molecule on endothelial cells were assessed by different means.

Preparation of HUVECs for further testing. Human umbilical cord was obtained from healthy new born with the consent form from the parents under the “Etablissement Francais du Sang” (Bordeaux, France) and HUVECs were isolated as previously described [25]. HUVECs were grown between passages 3 and 8 in Iscove`s Modified Dulbecco`s Medium (IMDM; Gibco, Thermo Fisher Scientific), containing 20 % fetal bovine serum (FBS; Lonza, Verviers, Belgium), 12 µg/mL endothelial cell growth factor supplement, and 90 µg/mL heparin (ECGS/H 0.4% (v/v); PromoCell, Heidelberg, Germany).

Migration test. Scratch migration assays were performed in 6 well plates, coated with 0.2 % gelatin (Sigma-Aldrich, saint Quentin Fallavier, France). Cells were seeded at 50,000 cells/cm² in 6 wells with the EBM2 media (Lonza, 00190860) containing 10 % FBS without

growth factors for 24 h. Wells containing confluent monolayer of HUVECs were then washed with Hanks balanced salt solution (HBSS, Gibco, Courtaboeuf, France) and a straight-line scratch was made using a 100 μ L pipette tip. The wells were gently washed with HBSS to remove detached cells and debris. 2 mL of positive control (Lonza, CC-3202, optimized for efficient endothelial cell proliferation), test (containing the tested compound GN-1 at a concentration of 1 mM in EBM2-10% FBS), and negative control (EBM2 medium containing 10% FBS) media were added to the wells. The closure of scratch was monitored by time lapse videomicroscopy with a frame rate of 10/min for 18 h in Etaluma Lumascope 720. The Etaluma software was used to generate the movies and to quantify the speed of wound closure.

Proliferation test. Proliferation analysis was performed at different concentrations of the compound GN-1 (2, 10, 20, 50, 100, 500, and 1000 μ M diluted in EBM2 medium + 10% FBS). HUVECs were seeded on 24 well plates at a low density of 10,000 cells/cm². The cells were cultured using EBM2 medium containing 10% FBS without any growth factors as basal medium supplemented or not with active compound, while the positive control medium was the complete EGM-2MV medium. To assess the proliferation on day 1 and 7, neutral red assays were performed as described for the cytotoxicity study (see paragraph 2.4).

2.6. *In vivo* experiments

Subcutaneous injection of hydrogels into mice. All animal studies were carried out in accredited animal facilities at the University of Bordeaux (accreditation number: A33-063-917) and approved by the animal ethical committee of Bordeaux. The four different hydrogels were prepared as described above and introduced while they were still in the liquid phase in 1 mL syringes. Ten-week-old OF-1 female mice (Charles Rivers, France, 35 g) were then anaesthetized using 4.5% isoflurane gas and maintained throughout surgery at 2.5% isoflurane with a face mask and depilated before surgery. The hydrogels (100 μ L) were injected subcutaneously using 21-gauge needle bilaterally on the dorsal side of the animals (1 hydrogel/side).

In vivo toxicity assays. Hepatocellular, cardiac and renal injury that might result from the toxicity of implanted hydrogels was assessed by measuring the serum concentrations of alanine aminotransferase (ALT, Activity Assay Kit, Sigma-Aldrich, ref MAK052), aspartate aminotransferase (AST, Activity Assay Kit, Sigma-Aldrich, ref MAK055), and lactate

dehydrogenase (LDH, Assay Kit, Abcam, ab102526). Just before surgery and 3, 7, and 21 d after hydrogel implantation, blood was collected from retro-orbital sinus, allowed to clot, and spun down to collect serum. Serum was used for analysis as recommended by the kit manufacturers.

Histology, staining and immunohistochemistry. Animals were sacrificed by cervical dislocation 1 and 3 weeks after hydrogel implantation. The hydrogels were harvested with the subcutaneous tissue and fixed in 4% paraformaldehyde (Antigenfix, Diapath, France) overnight at 4°C, followed by dehydration, embedding in paraffin, and sectioning by a microtome (5 µm thickness). The sections were either stained with Masson's trichrome or used for immunolabelling after antigen retrieval was performed by sodium citrate buffer 95°C for 30 min. Blood vessels in and around the hydrogels 21 d after implantation were identified by immunolabelling with rabbit anti-CD31 antibody (Abcam, ref ab28364 dilution:1/100) followed by incubation with HRP-conjugated anti-rabbit secondary antibody (Vector MP-7401, dilution:1/2). The inflammatory response to the biomaterials 21 d post-implantation was studied with the following primary antibodies: rabbit anti-CD68 (Abcam, ref ab1252012, 1/200), rabbit anti-CD206 (Abcam, ref ab64693, 1/500), and rabbit anti-CCR7 (Abcam, ref ab32527, dilution:1/100) followed by detection with Alexa568-conjugated goat anti-rabbit antibody. The fibrosis reaction around the hydrogels was detected by staining mesenchymal cells for vimentin (Cell Signal, ref 5741, 1/100), activated fibroblasts for the myofibroblasts marker α -smooth muscle actin (α -SMA) (α -SM-1, mouse IgG2a, a kind gift from Giulio Gabbiani, University of Geneva, Switzerland, dilution 1/50), and fibronectin (Santa Cruz, sc59826, 1/300). As secondary antibodies, we used goat anti-rabbit conjugated to TRITC (tetramethylrhodamine, Sigma Aldrich, T5268, dilution 1/100), goat antimouse IgG2a 647(Invitrogen, ref A21241, dilution 1/100), goat antimouse IgG1 FITC (Sigma Aldrich, dilution 1/200). All the images were acquired using a nanozoomer (Hamamatsu, Nanozoomer 2.0 HT).

Chick Chorioallantoic membrane (CAM) assay. To assess the supposed angiogenic properties of the GN-1 compound, we used the CAM of chick embryos (*Gallus gallus*) (E.A.R.L. Morizeau, Dangers, France) that were incubated at 37°C and 70 % humidity to initiate fertilization. On day 3 of development, 3-5 mL of egg white was withdrawn by punctuating the air chamber with the syringe, and a window was made by cutting the eggshell and sealed with Durapore® tape. On day 13, prepared plastic rings (made from Nunc Thermanox® coverslips, diameter 13 mm and thickness 0.2 mm) were placed on the intact CAM. 20 µL of the molecule

GN-1 (concentration 1 mM in DMEM medium) or an equivalent volume of DMEM alone as control were deposited in the center of the plastic rings. The treatment was repeated the following day followed by photo documentation (day 14). On day 17, the eggs were fixed by the addition of 2 mL of 4 % paraformaldehyde (Antigenfix, Diapath) for 30 min at room temperature. Imaging was performed with a stereomicroscope (Nikon SMZ800) using a digital camera (Nikon Coolpix 950). The images (1 per egg that showed almost all the surface inside the plastic ring) were scored for morphological changes of blood capillaries such as sprouting and tortuosity (0=normal, 1=overrepresented) by 5 observers using a blind test.

2.7. Statistical analyses

Data are presented as mean±s.d. Differences between groups were evaluated using Kruskal–Wallis (for at least three compared groups) and Mann–Whitney tests (for two compared groups) for non-parametric measures. To analyze hydrogel degradation over time, the Friedman test was used; the comparison of paired values was then performed with the use of the Wilcoxon matched-pair test. The Fisher exact test was used for the analysis of angiogenesis on CAM. Two-tailed *p* values less than 0.05 were considered significant.

3. RESULTS

3.1. Structure of molecules

To produce four different **self-assembled** hydrogels, LMWHs were stabilized by synthetic bioconjugates, which possess sugar, nucleoside, and lipid moieties covalently linked with triazole bridges. GNF was produced to contain a highly fluorinated and a carbohydrate moiety linked to the central thymidine, and three GNBA were produced as bolaamphiphilic structures with different functional groups. GNBA-1 and GNBA-2 were functionalized with one ureido group differing in one carbon atom whereas GNBA-3 contained one amide group (**Fig. 1, gray boxes**).

3.2. *In vitro* degradation/disassembly of LMWHs

Stability against degradation is critical for the clinical applicability of hydrogels. To assess the stability of the four hydrogels *in vitro*, the weight loss of the four LMWHs was measured after different periods of incubation in PBS at 37°C. After 21 d, the remaining weights were 65±4 % (GNF), 63±1 % (GNBA-1), 51±11 % (GNBA-2), and 55±2 % (GNBA-3). Friedman analysis of variance was performed (Fr=17.76, df 10,4, p<0.01), followed by Wilcoxon analysis to show that GNF degraded with slower kinetics compared with GNBA-2 ($p=0.007$) and GNBA-3 ($p=0.007$) (**Fig. 2**).

Next, we assessed the molecular nature of by-products of LMWH degradation using MALDI-TOF mass spectrometry after 21 d (**Fig. 1, arrows, and Suppl Fig. S2**). Samples obtained from all LMWH incubations exhibited molecular peaks (**P-1**) corresponding to the intact molecules with a mass corresponding to the calculated mass. Additional peaks (**P-2, P-3, P-4**) were observed in GNF, GNBA-1 and -3, corresponding to fragmentation products of the incubated hydrogels (**Suppl Fig. S2**). The first predicted fragmentation is due to the cleavage of the bond between the C1'-carbon of pentose ring and the N1'- nitrogen of the nucleobase (**Fig. 1, thick arrow (i), Peak 2** in mass spectrum); the second predicted fragmentation is due to the bond cleavage between bridged 5'-CH₂ and the pentose ring (**Fig. 1, thick arrow (ii), Peak 3** in the mass spectrum). Calculated mass and observed mass for the fragments due to predicted

cleavages are summarized in **Table 1** and **Figure 1**. GNBA-2 incubation delivered only minimal fragmentation peaks (**Suppl Fig. S2**), suggesting that weight loss of GNBA-2 hydrogels primarily resulted from the dissociation of building block molecules due to weak hydrogen bonding between ureido groups and due to less stable interactions between the triazole rings.

Three out of four LMWHs showed similar fragmentation patterns. Further mass spectrometry analysis revealed significant degradation of the molecules forming GNF and GNBA-3 hydrogels, whereas molecules forming hydrogels GNBA-1 and -2 were more stable or disassembled (**Suppl Fig S2**). The urea linkage (GNBA-1 and -2) underwent more stabilized self-assembly due to two hydrogen bonds compared to one hydrogen bond in the amide linkage (GNF and GNBA-3). This self-association of urea is much stronger than that of amides or urethanes, usually one hydrogen bond donors. However, for GNBA-2, ethylene bridges weaken hydrogen bonding between the ureido groups and might be responsible for the less stable aromatic interactions with the tetrazolium ring. The ethylene group flanking the tetrazolium ring and the ureido group is responsible for the disassociation of the GNBA-2 before the fragmentation during the degradation studies.

In conclusion, GNBA-2 and GNBA-3 exhibited moderately faster degradation kinetics than GNF and GNBA-1. Two main mechanisms of hydrogel degradation occurred: disassembly of bolaamphiphiles (GNBA-2, and to a lesser extent GNBA-1, and GNBA-3) and molecule hydrolysis (GNF, and to a lesser extent GNBA-3 and GNBA-1) (**Suppl Fig S2**).

3.3. Evaluation of LMWH cytotoxicity

To assess the potential cytotoxicity of leachables released by GNF, GNBA-1, -2, and -3, MTT and neutral red assays [26] were performed with mouse L929 cells, which are a recommended international standard for toxicity tests, with viability and metabolism above 70% being considered non-toxic (international standard ISO10993-5). Extracts were recovered during 3 successive days and incubated with cells for 24 h. In the presence of leachables of all LMWHs, the viability and metabolism of L929 were not significantly different from control medium

conditions and remained above 70% (**Fig. 3**, dashed line); in contrast, the toxic control (0.1% Triton X100) greatly affected the viability and metabolism of cells (**Fig. 3**).

In addition, cytotoxicity was assessed by direct contact (LMWHs put in inserts immersed in the cell culture) with both L929 cells and primary human adipose mesenchymal stromal cells (MSCs), which are potential therapeutic cells [27] (**Suppl. Fig. S3**). In the presence of all LMWHs, the viability of L929 cells and MSCs, and the metabolism of L929, were not significantly different from control medium conditions (**Fig. S3a, c, d**). In contrast, a moderate decrease of MSC metabolism to 60% and 70% was observed during the first 24 h of incubation with LMWHs as shown by the MTT assays (**Fig. S3b**). As MTT measures the mitochondrial activity, we conclude that during the first day after preparation, the hydrogels released a product with some inhibitory effect on mitochondrial activity.

To address potential *in vivo* toxicity of the LMWHs or their degradation by-products, we injected LMWHs subcutaneously in mice and measured after 3, 7, and 21 d: (1) serum markers such as alanine aminotransferase (ALT) and aspartate aminotransferase (AST) to indicate hepatocellular injury, (2) AST to indicate renal injury, and (3) lactate dehydrogenase (LDH) to indicate cardiac toxicity [28,29]. Time points were selected based on the *in vitro* degradation behavior of the hydrogels with 70-80% of the LMWH mass preserved after 3 d and degradation to 35% and 50% after 21 d (**Fig. 2**). None of the LMWH generated significant variation in serum hepatic function markers alanine aminotransferase (ALT) and aspartate aminotransferase (AST) or the cardiac toxicity marker LDH compared with serum levels in non-injected control mice (**Suppl. Fig. S4**). Collectively, these results demonstrate that degradation products of our **four** LMWHs did not induce hepato-, renal, or cardiotoxicity.

3.4. LMWHs do not elicit a strong FBR

Adsorption of proteins at the surface of biomaterials is the initial step in triggering a FBR. To assess protein binding capacity, LMWHs were incubated *in vitro* in BSA solution at 37°C and the amount of adsorbed protein was measured after 2 h (**Fig. 4**). GNBA-3 showed significantly higher protein adsorption ($118\pm 21\mu\text{g}/\text{cm}^2$) compared to GNF ($60\pm 3\mu\text{g}/\text{cm}^2$, $p=0.05$, 2-tailed). GNBA-1 ($78\pm 6\mu\text{g}/\text{cm}^2$) and GNBA-2 ($88\pm 17\mu\text{g}/\text{cm}^2$) had intermediate BSA adsorption levels; hydrogels incubated without BSA produced no substantial signal (**Fig. 4**).

To characterize tissue morphology and FBR, LMWHs and surrounding tissue were harvested 7 and 21 d following subcutaneous injection and *in situ* gelation. Collagen accumulation, degradation pattern, cell infiltration, and angiogenesis were then analyzed in histological sections (**Fig. 5**). Masson's trichrome blue-stained but sparse collagen fibrils were observed throughout the implant interior but disappeared after the degradation of LMWHs without forming scar tissue (**Fig. 5**). The smaller amount of gel remaining after 21 d confirmed the *in vitro* observations that GNBA-2 was degrading faster than GNF and GNBA-1, whereas GNBA-3 showed intermediate degradation kinetics (**Fig. 5**). Fluorescence staining of cell nuclei with DAPI was performed to quantify cell infiltration of LMWH (**Suppl. Fig. S6**). In the portions of remaining hydrogels, we observed a significantly higher cell infiltration in GNBA-3 (348 ± 58 cells/ 0.5 mm^2 , $p=0.006$) and GNBA-2 (399 ± 28 cells/ 0.5 mm^2 , $p=0.006$) compared to GNF (145 ± 32 cells/ 0.5 mm^2). GNBA-1 exhibited an intermediate quantity of infiltrated cells (245 ± 18 cells/ 0.5 mm^2); **cells that infiltrated GNF** were mostly confined to the hydrogel border with only very few cells invading the hydrogel center. In contrast, cells infiltrated GNBA-1 evenly, including the hydrogel center (**Suppl. Fig. S6**).

To investigate macrophage recruitment and **activation** phenotype, we used CD68 as a pan-macrophage marker, CCR7 as a pro-inflammatory marker (M1) and CD206 as a marker for immuno-modulatory macrophages (M2) [6] (**Fig. 6**). CCR7-positive cells populated the interior all LMWHs, most densely in GNBA-3 and GNBA-2 gels, whereas CD206 positive cells remained confined to the periphery of all hydrogels (**Fig. 6a**, hydrogel limits shown by a dashed line). To further investigate the formation of granulation tissue around hydrogels and to analyze the degree of fibrosis, tissue sections were stained for vimentin and α -SMA as markers of fibroblasts and myofibroblasts, respectively. Only few vimentin-positive cells were detected in

the hydrogel periphery and no stromal cells stained positive for α -SMA, in contrast to α -SMA- and desmin-double-positive vascular smooth muscle cells (**Fig. 6b**). These data show that LMWHs did neither trigger an FBR nor a fibrotic reaction.

3.5. Analysis of proangiogenic properties of LMWHs

During tissue regeneration, development of neo-vessels is of major importance. To assess angiogenesis, we immunostained endothelial cells for CD31 21 d post-injection when LMWHs were mostly degraded or disassembled. CD31-positive cells with luminal structure (**Fig. 6c**, arrows) were observed in hydrogel proximity, and in the tissue that replaced the degrading LMWHs. CD31-positive endothelial cells were not found inside the hydrogels, showing that non-degraded LMWHs are not susceptible to blood vessel ingress. In an area of 0.2 mm² around GNBA-2 hydrogels, we counted 2.7-fold and 2.1-fold reduced numbers of blood vessels (bv) (3.0 ± 0.3 bv/0.2 mm²) compared to GNBA-3 (8.0 ± 0.7 bv/0.2 mm², $p=0.009$) and GNF (6.1 ± 1.1 bv/0.2 mm², $p=0.009$), respectively (**Fig. 6d**). Implantation of GNBA-1 hydrogels resulted in an intermediate angiogenic response (4.3 ± 0.4 bv/0.2 mm², $p>0.05$) (**Fig. 6d**). Thus GNF, GNBA-1, and GNBA-3 were associated with higher angiogenesis than GNBA-2.

Because GNF, GNBA-1, and GNBA-3 (but not GNBA-2) also released glyconucleoside (GN)-1 as a common product in *in vitro* degradation assays (peak 3, **Suppl Fig. S2**), we hypothesized that GN-1 has angiogenic properties. To test this hypothesis, GN-1 was chemically synthesized (**Fig. 7a**, **Suppl. Fig. S1**) and first tested for its effect on proliferation and migration of human umbilical vein endothelial cells (HUVECs), commonly used *in vitro* models of angiogenesis. In basal medium (EGM2 containing 10% fetal calf serum) HUVEC were able to survive but did not proliferate (not shown). GN-1 added in different concentrations did not induce HUVEC proliferation after 1 or 7 d culture in basal medium cultures (**Fig. 7b**). In contrast, significantly higher proliferation was measured by culturing HUVECs in endothelial cell growth medium used as a positive control (in basal medium cultures (6.7-fold, $p=0.0008$) (**Fig. 7b**). Addition of GN-1 (1 mM) to HUVEC monolayers that have been scratched in basal medium moderately increased HUVEC

migration into the gap without reaching significance (film in **Fig. S7** in supplementary materials, **Fig. 7c, d**).

Finally, we used the chorioallantoic membrane (CAM) *in vivo* model to assess the angiogenic potential of GN-1 (1 mM). We added the first dose of GN-1 on embryonic day 13 after the beginning of egg incubation and a second dose at day 14; DMEM was used as control. The angiogenic response was evaluated on day 17 based on vessel sprouting, and tortuosity (**Fig. 7e**). CAMs exhibited either normal vasculature (**Fig. 7e**, 1st column), a pattern with massive sprouting (**Fig. 7e**) and/or a pattern with many tortuous capillaries (**Fig. 7e**). Quantification of eggs with or without sprouting, and/or tortuous vessels showed that GN-1 treated CAMs exhibited more sprouting and tortuous vessels compared to control CAMs (**Fig. 7f**). Consistently, CAMs without sprouting or without tortuous vessels were more frequent in the control group (**Fig. 7f**). The differences between treated and non-treated CAMs were statistically significant: $p=0.0046$ and $p=0.0195$, for the sprouting and tortuous vessel effects, respectively (**Fig. 7f**, Fisher's exact test).

4. DISCUSSION

Hydrogels are receiving increasing attention to be used in various biomedical applications because their tunable properties offer a large range of potential developments. Yet, only a few hydrogels have entered the clinic drug delivery systems, wound dressings, and contact lenses [30]. The medical suitability of hydrogels largely depends on degradation rates, and effects on host tissue and cells at the site of implantation or injection. The possibility to form hydrogels from the self-assembly of small molecules provide additional properties compared to gels formed with polymeric materials: as pointed by Draper and Adams [31], the final properties of LMWHs (viscosity, fiber organization) are process-dependent, giving access to properties with the same molecules.

Here, we produced and analyzed four hydrogels obtained by the self-assembly of GNF and GNBA for properties that are key in medical applications. All four LMWHs share a glyco-nucleo-lipid moiety consisting of a thymidine block linked to a glucose molecule by a triazole heterocycle. They differ in two ways: GNF is single chain amphiphile, whereas the GNBA feature bolaamphiphilic structures, consisting of two GNs symmetrically separated by a hydrocarbon chain. The three GNBA differ in hydrocarbon chains or chemical functions (amide, urea). Interestingly, all four molecules stabilize into hydrogels at low concentrations (< 2% w/v) within less than one hour in aqueous media, and within less than 2 min when injected subcutaneously. Of note, all four hydrogels are fully injectable in a semi-liquid state to quickly form gels *in situ*. This property can be explained by the strain induced by extrusion through the needle and allows for easy subcutaneous injection. Injectability and *in situ* gel formation minimize invasive surgical procedures, a competitive advantage for therapeutic applications [9]. Previous studies have shown that the self-assembly of GNBA creates unique hydrogel supramolecular assemblies featuring fast gelation kinetics, high elastic moduli, thixotropy, and thermal reversibility. With these viscoelastic properties all four gels range among the ‘intermediate hard gels’, above ‘weak’ collagen gels, but below the commonly used polyethylene glycol (PEG)-based hydrogels. None of our four LMWHs exhibited any toxicity in cell culture tests with L929 cells or MSCs and no systemic toxicity when injected subcutaneously in mice. A small effect was measured on the mitochondrial activity of primary MSCs during the first 24 h.

Collectively, LMWHs and their degradation products are non-toxic and possibly safe for *in vivo* applications.

An overly strong FBR can prevent the proper functioning of implantable medical devices, the release of active compounds into the bloodstream, or the integration of a tissue engineering product [4,32]. The FBR is initiated by adsorption of proteins on the implanted material with a well-documented positive correlation between the degree of non-specific protein adsorption and the severity of inflammatory reaction. For instance, denaturation of fibrinogen due to adsorption to a material surface exposes hidden epitopes that recruit macrophages [33]. Minimizing non-specific protein adsorption is therefore an important challenge that can be overcome by hydrophilic materials. Indeed, the decrease of wettability of a surface increases the adsorption of BSA, fibrinogen and FXII [34]. **As hydrophilic materials, hydrogels are receiving a growing interest.** Our four LMWHs showed non-specific BSA adsorptions that were in the range of 60-120 $\mu\text{g}/\text{cm}^2$, **comparable to other hydrogels [35] or anti-fouling surfaces [36], whose non-specific protein adsorption was assessed under comparable conditions.** Highest BSA adsorption was observed with GNBA-3 and lowest values (2-fold lower) were obtained with GNF gels (**Fig. 4**), suggesting enhanced biocompatibility of GNF over GNBA-3. The different protein adsorption capacities correlated well with the levels of *in vivo* infiltration by macrophages. GNF and GNBA-1 LMWHs exhibit limited cell infiltration, whereas GNBA-2 and GNBA-3 were infiltrated by pro-inflammatory macrophages. Moreover, macrophage infiltration rates correlated with the degree and rate of gel degradation. GNBA-2 and GNBA-3 with highest cell infiltrations degraded with fastest rates. Our analyses further suggest that gel degradation is essentially cell-mediated, and that the spontaneous degradation observed *in vitro* plays a minor role. Thus, slowly degrading GNF and GNBA-1 are well suited for tissue engineering applications, whereas rapidly degrading GNBA-2 and GNBA-3 are more adapted to drug delivery applications, in which drug release could be coupled to gel degradation/disassembly.

Macrophage recruitment and phenotypic switch (polarization) are essential factors in controlling the progression of the FBR into fibrosis [7]. **After implantation, chemoattractant cytokines attract blood circulating monocytes that first differentiate to macrophages with a pro-inflammatory 'M1' phenotype [6,7]. Depending on the material and on microenvironment cues,**

macrophages increasingly attain immuno-modulatory and remodeling phenotypes, that are part of a 'M2' phenotype spectrum [6–8]. The population of immuno-modulatory M2 phenotypes typically culminates after 7 to 10 d around biomaterials with good biocompatibility properties. Consistently, macrophage depletion was shown to result in increased fibrotic capsule thickness around implants [37]. While the M1/M2 paradigm is a simplified view on the macrophage polarization spectrum, M1 to M2 phenotype switch is considered important for the success of material implantations, including the development of a blood vessel network. *In vitro*, pro-inflammatory M1 macrophages express high levels of VEGF that favors endothelial cell sprouting, whereas IL-4/IL-13-polarized M2a macrophages in culture express high levels of PDGF-BB that recruits pericytes to stabilize the neo-vessels [38]. Conversely, IL-10-activated *in vitro* M2c macrophages express increased levels of MMP9 that allows for the vessel remodeling [43]. Compared to other biomaterials like poly(lactic acid) [39] or chitosan [40] that are invaded by M1- and M2-like macrophages, the phenotypes that were observed in our hydrogels were highly contrasted: macrophages that had invaded the materials almost exclusively expressed CCR7, a cell receptor considered as a marker essentially expressed by M1 macrophages. At the same time (three weeks after implantation), macrophages present in the surrounding tissue mostly expressed CD206, a receptor associated with an alternative activation phenotype. In agreement with the concept that the presence of M2 macrophages is associated with a better *in vivo* biointegration [41], we observed here that biointegration was optimal for all four LMWHs, as no sign of any fibrous capsule formation was evidenced after 3 weeks (**Fig. 6b**). **These data contrast with the development of fibrous capsules with most implanted biomaterials [42–45], such as PEG hydrogels recognized as gold standard biomaterials [46].** Interestingly, the hydrogel invasion by macrophages that remain with a proinflammatory M1 phenotype after 3 weeks may be suggestive of biomaterials promoting the formation of a thick fibrous capsule, as mentioned in many articles and reviews. However, this was not the case with any of the four tested LMWHs. The role of macrophages in the fibrotic process regulation is far from clear [47], but the main characteristic of FBR to biomaterials seems to be macrophages exhibiting a mixed M1/M2 phenotype [48]. Thus, it seems that the absence of fibrous capsule around the four hydrogels is related to the presence of both M1 and M2 macrophages in the LMWH vicinity rather than to the proinflammatory macrophages inside the hydrogels. Further experiments will be needed to identify whether the infiltrated M1 macrophages are involved in the integration of the

biomaterials, in parallel with its degradation. In addition, although no fibrosis was observed where the hydrogels were degrading (particularly GNBA-2 which was already largely degraded after 3 weeks), a longer implantation time such as 2 to 3 months could be performed to confirm the absence of a fibrotic tissue after total LMWH degradation. **Whatever the mechanism responsible for the absence of fibrous capsule around the four types of gels, this property is quite unusual and points these LMWGS as potential therapeutic tools for various applications.**

During material biodegradation and tissue remodeling, the development of a vascular network is of major importance. In this context, we found that three out of four hydrogels gave the same degradation by-product *in vitro* (a glyconucleoside, *i.e.* glucose covalently bound to thymidine, **Fig. 7a**) and that these three hydrogels induced a better vascularization three weeks after subcutaneous implantation (**Fig. 6c, d**). We hypothesized that this glyconucleoside might have angiogenic properties. Its chemical synthesis confirmed *in vitro* that this compound seemed to be able to improve endothelial cell migration in a scratch assay, although at a low level (**Fig. 7d**, no significant difference). In a culture experiment with HUVECs grown in a basal medium, we confirmed that no cytotoxicity was observed but that this compound did not favor cell proliferation.

The problem of the relative contributions of proliferation and migration is very important for the understanding of angiogenesis regulation and some studies identified agents that can specifically target migration. Along this line, serpin-derived peptides have shown anti-angiogenic effects by sustaining the phosphorylation of the focal adhesion kinase, thus diminishing specifically cell migration [49]. Moreover, Norton and Popel used a 3D model of angiogenesis well-characterized into which tip cell migration, endothelial cell proliferation and sprouting were simulated [50]. They were able to predict that the proliferation rate has a greater effect on the spreading and extent of the vascular growth in comparison to the migration rate. Based on our *in vitro* assays, we can take advantage of the fact that our molecule promotes slightly migration to combine it with a scaffold designed for tissue engineering. Thus, it can be incorporated advantageously into bioprinting methods to help the structuration of a vascular network [51,52]. The tortuosity of neo-vessels that was evidenced with the *in vivo* CAM model treated with the active compound (**Fig. 7e**) is evocative of an active angiogenic process. Indeed,

such tortuosity has been observed for a long time in the presence of VEGF and is shown to be also associated with local hypoxia [53,54]. In our experiments, among 23 CAM control assays (only the vehicle was added), only 3 CAM vascular networks showed some tortuosity that may be associated with local hypoxia induced by the plastic ring used to limit the area receiving the medium. In contrast, the addition of the active compound induced the formation of these tortuous vessels in half of the group (9/19) (**Fig. 7f**). Chong *et al.* [55] demonstrated in a mouse model of ear wound healing, that tortuous microvessels were detected already 3 d after wound and peaked at 17 d post-wound, and that the alteration of blood flow promoted sprouting in these regions, thus generating efficient angiogenesis in the area surrounding the wound.

The structural similarity of the degradation product with nucleoside may suggest that the compound exerts its action as an agonist of P2Y receptors. Several studies have shown that AMP, Adenosine and ATP stimulate angiogenesis via receptors on endothelial cells, and that this effect mainly involves the stimulation of cell migration [56,57]. Although further studies are required to investigate the mechanisms responsible for favored vascularization, both *in vitro* with HUVECs and *in vivo* in mice, our data clearly demonstrate the angiogenic properties of three out of four hydrogels. The question remains whether the GNBA and GNF show the same angiogenic properties as intact molecules, as GNBA-2 that has a molecular formula near GNBA-1's one but was not subjected to hydrolysis *in vitro*, was inducing angiogenesis less efficiently.

In conclusion, the present article presents four hydrogels formed with self-assembling of low molecular weight hydrogels, that degrade with different kinetics when subcutaneously implanted, and that do not induce the formation of any fibrous capsule; three among these four hydrogels promote angiogenesis by the release of a degradation by-product with angiogenic properties. We suggest that GNF and GNBA-1 are promising candidates for applications in tissue engineering, whereas GNBA-3 could be efficiently used for drug release applications.

COMPLIANCE WITH ETHICAL STANDARDS

Declaration of Competing Interest. The authors declare that they have no conflict of interest.

Ethical Approval. All applicable international, national, and institutional guidelines for the care and use of animals were followed. All procedures performed in studies involving animals were in accordance with the ethical standards of the institution or practice at which the studies were conducted (animal experimentation permission APAFIS#4375-2016030408537165).

ACKNOWLEDGMENTS

This work was supported by a grant from ANR (Bio3, ANR-16-CE19-0001-01). SKR and NB received doctoral and postdoctoral fellowships from LabEx AMADEus, respectively (ANR-10-LABX-0042-AMADEUS). The research of BH is supported by the Canadian Institutes of Health Research (CIHR), Foundation Grant #375597 and the Canada Foundation for Innovation and Ontario Research Fund (CFI/ORF), grants #26653 and #36050. We would like to thank the animal house A1 facility (University of Bordeaux).

SUPPLEMENTARY DATA

Supplementary material associated with this article can be found, in the online version, at doi:

BIBLIOGRAPHIC REFERENCES

- [1] B. Lei, B. Guo, K.J. Rambhia, P.X. Ma, Hybrid polymer biomaterials for bone tissue regeneration, *Frontiers of Medicine*. (2018). <https://doi.org/10.1007/s11684-018-0664-6>.
- [2] J. Saliba, A. Daou, S. Damiati, J. Saliba, M. El-Sabban, R. Mhanna, Development of Microplatforms to Mimic the In Vivo Architecture of CNS and PNS Physiology and Their Diseases, *Genes*. 9 (2018) 285. <https://doi.org/10.3390/genes9060285>.
- [3] E. Anitua, P. Nurden, R. Prado, A.T. Nurden, S. Padilla, Autologous fibrin scaffolds: When platelet- and plasma-derived biomolecules meet fibrin, *Biomaterials*. 192 (2019) 440–460. <https://doi.org/10.1016/j.biomaterials.2018.11.029>.
- [4] J.M. Anderson, A. Rodriguez, D.T. Chang, Foreign body reaction to biomaterials, *Semin. Immunol.* 20 (2008) 86–100. <https://doi.org/10.1016/j.smim.2007.11.004>.
- [5] B.J. Kwee, D.J. Mooney, Manipulating the Intersection of Angiogenesis and Inflammation, *Ann Biomed Eng.* 43 (2015) 628–640. <https://doi.org/10.1007/s10439-014-1145-y>.
- [6] A. Mantovani, A. Sica, S. Sozzani, P. Allavena, A. Vecchi, M. Locati, The chemokine system in diverse forms of macrophage activation and polarization, *Trends in Immunology*. 25 (2004) 677–686. <https://doi.org/10.1016/j.it.2004.09.015>.
- [7] B.N. Brown, B.M. Sicari, S.F. Badylak, Rethinking Regenerative Medicine: A Macrophage-Centered Approach, *Front. Immunol.* 5 (2014). <https://doi.org/10.3389/fimmu.2014.00510>.
- [8] S. Gordon, P.R. Taylor, Monocyte and macrophage heterogeneity, *Nat Rev Immunol.* 5 (2005) 953–964. <https://doi.org/10.1038/nri1733>.
- [9] Y. Sun, D. Nan, H. Jin, X. Qu, Recent advances of injectable hydrogels for drug delivery and tissue engineering applications, *Polymer Testing*. 81 (2020) 106283. <https://doi.org/10.1016/j.polymertesting.2019.106283>.
- [10] J. Baillet, V. Desvergnès, A. Hamoud, L. Latxague, P. Barthélémy, Lipid and Nucleic Acid Chemistries: Combining the Best of Both Worlds to Construct Advanced Biomaterials, *Advanced Materials*. 30 (2018) 1705078. <https://doi.org/10.1002/adma.201705078>.
- [11] K.J. Skilling, F. Citossi, T.D. Bradshaw, M. Ashford, B. Kellam, M. Marlow, Insights into low molecular mass organic gelators: a focus on drug delivery and tissue engineering applications, *Soft Matter*. 10 (2014) 237–256. <https://doi.org/10.1039/C3SM52244J>.
- [12] M.G.F. Angelerou, P.W.J.M. Frederix, M. Wallace, B. Yang, A. Rodger, D.J. Adams, M. Marlow, M. Zelzer, Supramolecular Nucleoside-Based Gel: Molecular Dynamics Simulation and Characterization of Its Nanoarchitecture and Self-Assembly Mechanism, *Langmuir*. 34 (2018) 6912–6921. <https://doi.org/10.1021/acs.langmuir.8b00646>.
- [13] M.G.F. Angelerou, B. Yang, T. Arnold, J. Rawle, M. Marlow, M. Zelzer, Hydrophobicity of surface-immobilised molecules influences architectures formed *via* interfacial self-assembly of nucleoside-based gelators, *Soft Matter*. 14 (2018) 9851–9855. <https://doi.org/10.1039/C8SM01868E>.
- [14] R. Van Lommel, L.A.J. Rutgeerts, W.M. De Borggraeve, F. De Proft, M. Alonso, Rationalising Supramolecular Hydrogelation of Bis-Urea-Based Gelators through a Multiscale Approach, *ChemPlusChem*. 85 (2020) 267–276. <https://doi.org/10.1002/cplu.201900551>.
- [15] G. Godeau, J. Bernard, C. Staedel, P. Barthélémy, Glycosyl–nucleoside–lipid based supramolecular assembly as a nanostructured material with nucleic acid delivery capabilities,

- Chem. Commun. (2009) 5127. <https://doi.org/10.1039/b906212b>.
- [16] S. Ziane, S. Schlaubitz, S. Miraux, A. Patwa, C. Lalande, I. Bilem, S. Lepreux, B. Rousseau, J.-F. Le Meins, L. Latxague, P. Barthélémy, O. Chassande, A thermosensitive low molecular weight hydrogel as scaffold for tissue engineering, *Eur Cell Mater.* 23 (2012) 147–160; discussion 160. <https://doi.org/10.22203/ecm.v023a11>.
- [17] D. Jain, A. Karajic, M. Murawska, B. Goudeau, S. Bichon, S. Gounel, N. Mano, A. Kuhn, P. Barthélémy, Low-Molecular-Weight Hydrogels as New Supramolecular Materials for Bioelectrochemical Interfaces, *ACS Appl. Mater. Interfaces.* 9 (2017) 1093–1098. <https://doi.org/10.1021/acsami.6b12890>.
- [18] M. Maisani, K.R. Sindhu, M. Fenelon, R. Siadous, S. Rey, D. Mantovani, O. Chassande, Prolonged delivery of BMP-2 by a non-polymer hydrogel for bone defect regeneration, *Drug Deliv. and Transl. Res.* 8 (2018) 178–190. <https://doi.org/10.1007/s13346-017-0451-y>.
- [19] M. Maisani, S. Ziane, C. Ehret, L. Levesque, R. Siadous, J. Le Meins, P. Chevallier, P. Barthélémy, H. De Oliveira, J. Amédée, D. Mantovani, O. Chassande, A new composite hydrogel combining the biological properties of collagen with the mechanical properties of a supramolecular scaffold for bone tissue engineering, *J Tissue Eng Regen Med.* 12 (2018). <https://doi.org/10.1002/term.2569>.
- [20] M.A. Ramin, K.R. Sindhu, A. Appavoo, K. Oumzil, M.W. Grinstaff, O. Chassande, P. Barthélémy, Cation Tuning of Supramolecular Gel Properties: A New Paradigm for Sustained Drug Delivery, *Adv. Mater.* 29 (2017) 1605227. <https://doi.org/10.1002/adma.201605227>.
- [21] L. Latxague, M.A. Ramin, A. Appavoo, P. Berto, M. Maisani, C. Ehret, O. Chassande, P. Barthélémy, Control of Stem-Cell Behavior by Fine Tuning the Supramolecular Assemblies of Low-Molecular-Weight Gelators, *Angew. Chem. Int. Ed.* 54 (2015) 4517–4521. <https://doi.org/10.1002/anie.201409134>.
- [22] L. Latxague, A. Patwa, E. Amigues, P. Barthélémy, Glycosyl-Nucleolipids as New Bioinspired Amphiphiles, *Molecules.* 18 (2013) 12241–12263. <https://doi.org/10.3390/molecules181012241>.
- [23] G. Godeau, C. Brun, H. Arnion, C. Staedel, P. Barthélémy, Glycosyl-nucleoside fluorinated amphiphiles as components of nanostructured hydrogels, *Tetrahedron Letters.* 51 (2010) 1012–1015. <https://doi.org/10.1016/j.tetlet.2009.12.042>.
- [24] M.A. Ramin, L. Latxague, K.R. Sindhu, O. Chassande, P. Barthélémy, Low molecular weight hydrogels derived from urea based-bolaamphiphiles as new injectable biomaterials, *Biomaterials.* 145 (2017) 72–80. <https://doi.org/10.1016/j.biomaterials.2017.08.034>.
- [25] H. Li, R. Daculsi, M. Grellier, R. Bareille, C. Bourget, J. Amedee, Role of neural-cadherin in early osteoblastic differentiation of human bone marrow stromal cells cocultured with human umbilical vein endothelial cells, *American Journal of Physiology-Cell Physiology.* 299 (2010) C422–C430. <https://doi.org/10.1152/ajpcell.00562.2009>.
- [26] G. Repetto, A. del Peso, J.L. Zurita, Neutral red uptake assay for the estimation of cell viability/cytotoxicity, *Nat Protoc.* 3 (2008) 1125–1131. <https://doi.org/10.1038/nprot.2008.75>.
- [27] D. Lo Furno, G. Mannino, V. Cardile, R. Parenti, R. Giuffrida, Potential Therapeutic Applications of Adipose-Derived Mesenchymal Stem Cells, *Stem Cells Dev.* 25 (2016) 1615–1628. <https://doi.org/10.1089/scd.2016.0135>.
- [28] A. Wijekoon, N. Fountas-Davis, N.D. Leipzig, Fluorinated methacrylamide chitosan hydrogel systems as adaptable oxygen carriers for wound healing, *Acta Biomaterialia.* 9 (2013) 5653–5664. <https://doi.org/10.1016/j.actbio.2012.10.034>.
- [29] P.A. Markov, D.S. Khramova, K.V. Shumikhin, I.R. Nikitina, V.S. Beloserev, E.A.

- Martinson, S.G. Litvinets, S.V. Popov, Mechanical properties of the pectin hydrogels and inflammation response to their subcutaneous implantation, *J. Biomed. Mater. Res.* 107 (2019) 2088–2098. <https://doi.org/10.1002/jbm.a.36721>.
- [30] E. Caló, V.V. Khutoryanskiy, Biomedical applications of hydrogels: A review of patents and commercial products, *European Polymer Journal.* 65 (2015) 252–267. <https://doi.org/10.1016/j.eurpolymj.2014.11.024>.
- [31] E.R. Draper, T.O. McDonald, D.J. Adams, A low molecular weight hydrogel with unusual gel aging, *Chem. Commun. (Camb.).* 51 (2015) 6595–6597. <https://doi.org/10.1039/c5cc01334h>.
- [32] R. Klopffleisch, F. Jung, The pathology of the foreign body reaction against biomaterials: Foreign Body Reaction to Biomaterials, *J. Biomed. Mater. Res.* 105 (2017) 927–940. <https://doi.org/10.1002/jbm.a.35958>.
- [33] W.J. Hu, J.W. Eaton, T.P. Ugarova, L. Tang, Molecular basis of biomaterial-mediated foreign body reactions, *Blood.* 98 (2001) 1231–1238.
- [34] L.-C. Xu, C.A. Siedlecki, Effects of surface wettability and contact time on protein adhesion to biomaterial surfaces, *Biomaterials.* 28 (2007) 3273–3283. <https://doi.org/10.1016/j.biomaterials.2007.03.032>.
- [35] V. Huynh, A.D. D'Angelo, R.G. Wylie, Tunable degradation of low-fouling carboxybetaine-hyaluronic acid hydrogels for applications in cell encapsulation, *Biomed. Mater.* 14 (2019) 055003. <https://doi.org/10.1088/1748-605X/ab2bde>.
- [36] C. Xu, X. Hu, J. Wang, Y.-M. Zhang, X.-J. Liu, B.-B. Xie, C. Yao, Y. Li, X.-S. Li, Library of Antifouling Surfaces Derived From Natural Amino Acids by Click Reaction, *ACS Appl. Mater. Interfaces.* 7 (2015) 17337–17345. <https://doi.org/10.1021/acsami.5b04520>.
- [37] R.A. Bank, J. Zandstra, H. Room, A.H. Petersen, S.M. van Putten, Biomaterial Encapsulation Is Enhanced in the Early Stages of the Foreign Body Reaction During Conditional Macrophage Depletion in Transgenic Macrophage Fas-Induced Apoptosis Mice, *Tissue Engineering Part A.* 23 (2017) 1078–1087. <https://doi.org/10.1089/ten.tea.2016.0499>.
- [38] K.L. Spiller, R.R. Anfang, K.J. Spiller, J. Ng, K.R. Nakazawa, J.W. Daulton, G. Vunjak-Novakovic, The role of macrophage phenotype in vascularization of tissue engineering scaffolds, *Biomaterials.* 35 (2014) 4477–4488. <https://doi.org/10.1016/j.biomaterials.2014.02.012>.
- [39] H. Oliveira, S. Catros, C. Boiziau, R. Siadous, J. Marti-Munoz, R. Bareille, S. Rey, O. Castano, J. Planell, J. Amédée, E. Engel, The proangiogenic potential of a novel calcium releasing biomaterial: Impact on cell recruitment, *Acta Biomaterialia.* 29 (2016) 435–445. <https://doi.org/10.1016/j.actbio.2015.10.003>.
- [40] D.P. Vasconcelos, A.C. Fonseca, M. Costa, I.F. Amaral, M.A. Barbosa, A.P. Águas, J.N. Barbosa, Macrophage polarization following chitosan implantation, *Biomaterials.* 34 (2013) 9952–9959. <https://doi.org/10.1016/j.biomaterials.2013.09.012>.
- [41] J. Barthes, C. Dollinger, C.B. Muller, U. Liivas, A. Dupret-Bories, H. Knopf-Marques, N.E. Vrana, Immune Assisted Tissue Engineering via Incorporation of Macrophages in Cell-Laden Hydrogels Under Cytokine Stimulation, *Front Bioeng Biotechnol.* 6 (2018) 108. <https://doi.org/10.3389/fbioe.2018.00108>.
- [42] A.D. Lynn, A.K. Blakney, T.R. Kyriakides, S.J. Bryant, Temporal progression of the host response to implanted poly(ethylene glycol)-based hydrogels, *J. Biomed. Mater. Res.* 96A (2011) 621–631. <https://doi.org/10.1002/jbm.a.33015>.
- [43] L.E. Jansen, L.D. Amer, E.Y.-T. Chen, T.V. Nguyen, L.S. Saleh, T. Emrick, W.F. Liu, S.J. Bryant, S.R. Peyton, Zwitterionic PEG-PC Hydrogels Modulate the Foreign Body Response

- in a Modulus-Dependent Manner, *Biomacromolecules*. 19 (2018) 2880–2888.
<https://doi.org/10.1021/acs.biomac.8b00444>.
- [44] Y. Qian, L. Li, Y. Song, L. Dong, P. Chen, X. Li, K. Cai, O. Germershaus, L. Yang, Y. Fan, Surface modification of nanofibrous matrices via layer-by-layer functionalized silk assembly for mitigating the foreign body reaction, *Biomaterials*. 164 (2018) 22–37.
<https://doi.org/10.1016/j.biomaterials.2018.02.038>.
- [45] N.G. Welch, S. Mukherjee, M.A. Hossain, P. Praveen, J.A. Werkmeister, J.D. Wade, R.A.D. Bathgate, D.A. Winkler, H. Thissen, Coatings Releasing the Relaxin Peptide Analogue B7-33 Reduce Fibrotic Encapsulation, *ACS Appl. Mater. Interfaces*. 11 (2019) 45511–45519.
<https://doi.org/10.1021/acsami.9b17859>.
- [46] A.W. Bridges, A.J. García, Anti-Inflammatory Polymeric Coatings for Implantable Biomaterials and Devices, *J Diabetes Sci Technol*. 2 (2008) 984–994.
<https://doi.org/10.1177/193229680800200628>.
- [47] C.E. Witherel, D. Abeyayehu, T.H. Barker, K.L. Spiller, Macrophage and Fibroblast Interactions in Biomaterial-Mediated Fibrosis, *Adv. Healthcare Mater.* (2019) 1801451.
<https://doi.org/10.1002/adhm.201801451>.
- [48] T. Yu, W. Wang, S. Nassiri, T. Kwan, C. Dang, W. Liu, K.L. Spiller, Temporal and spatial distribution of macrophage phenotype markers in the foreign body response to glutaraldehyde-crosslinked gelatin hydrogels, *Journal of Biomaterials Science, Polymer Edition*. 27 (2016) 721–742. <https://doi.org/10.1080/09205063.2016.1155881>.
- [49] J.E. Koskimaki, E.V. Rosca, C.G. Rivera, E. Lee, W. Chen, N.B. Pandey, A.S. Popel, Serpin-derived peptides are antiangiogenic and suppress breast tumor xenograft growth, *Transl Oncol*. 5 (2012) 92–97.
- [50] K.-A. Norton, A.S. Popel, Effects of endothelial cell proliferation and migration rates in a computational model of sprouting angiogenesis, *Sci Rep*. 6 (2016) 36992.
<https://doi.org/10.1038/srep36992>.
- [51] J.-M. Bourget, O. Kérourédan, M. Medina, M. Rémy, N.B. Thébaud, R. Bareille, O. Chassande, J. Amédée, S. Catros, R. Devillard, Patterning of Endothelial Cells and Mesenchymal Stem Cells by Laser-Assisted Bioprinting to Study Cell Migration, *BioMed Research International*. 2016 (2016) 1–7. <https://doi.org/10.1155/2016/3569843>.
- [52] M.D. Sarker, S. Naghieh, N.K. Sharma, L. Ning, X. Chen, Bioprinting of Vascularized Tissue Scaffolds: Influence of Biopolymer, Cells, Growth Factors, and Gene Delivery, *Journal of Healthcare Engineering*. 2019 (2019) 1–20. <https://doi.org/10.1155/2019/9156921>.
- [53] A. Saaristo, T. Veikkola, B. Enholm, M. Hytönen, J. Arola, K. Pajusola, P. Turunen, M. Jeltsch, M.J. Karkkainen, D. Kerjaschki, H. Bueler, S. Ylä-Herttuala, K. Alitalo, Adenoviral VEGF-C overexpression induces blood vessel enlargement, tortuosity, and leakiness but no sprouting angiogenesis in the skin or mucous membranes, *FASEB J*. 16 (2002) 1041–1049.
<https://doi.org/10.1096/fj.01-1042com>.
- [54] S. Lee, S.M. Jilani, G.V. Nikolova, D. Carpizo, M.L. Iruela-Arispe, Processing of VEGF-A by matrix metalloproteinases regulates bioavailability and vascular patterning in tumors, *The Journal of Cell Biology*. 169 (2005) 681–691. <https://doi.org/10.1083/jcb.200409115>.
- [55] D.C. Chong, Z. Yu, H.E. Brighton, J.E. Bear, V.L. Bautch, Tortuous Microvessels Contribute to Wound Healing via Sprouting Angiogenesis, *Arteriosclerosis, Thrombosis, and Vascular Biology*. 37 (2017) 1903–1912. <https://doi.org/10.1161/ATVBAHA.117.309993>.
- [56] S. Mühleder, C. Fuchs, J. Basílio, D. Szwarc, K. Pill, K. Labuda, P. Slezak, C. Siehs, J. Pröll, E. Priglinger, C. Hoffmann, W.G. Junger, H. Redl, W. Holnthoner, Purinergic P2Y2

receptors modulate endothelial sprouting, *Cell. Mol. Life Sci.* 77 (2020) 885–901.
<https://doi.org/10.1007/s00018-019-03213-2>.

[57] Z. Zhou, I. Chrifi, Y. Xu, J. Pernow, D.J. Duncker, D. Merkus, C. Cheng, Uridine adenosine tetraphosphate acts as a proangiogenic factor *in vitro* through purinergic P2Y receptors, *American Journal of Physiology-Heart and Circulatory Physiology.* 311 (2016) H299–H309. <https://doi.org/10.1152/ajpheart.00578.2015>.

FIGURE LEGENDS

Table 1. Degradation products analyzed by MALDI-TOF. The calculated and observed masses of the degradation products shown in Fig. 1 are given. The mass spectra are available in supplementary figure S2. **BLACK & WHITE FIGURE**

Figure 1. Chemical structures of GNF, and GNBA and analysis of *in vitro* degradation. GNF and GNBA-3 contain an amide group, whereas GNBA-1 and GNBA-2 contain a urea group (highlighted in gray). The degradation products released in PBS after a 21 d incubation at 37°C were analyzed by MALDI-TOF mass spectrometry (Suppl. Fig. S2). The positions of hypothetical hydrolysis are shown by arrows (cleavage sites (i) and (ii)). Calculated and observed masses are given in Table 1. **BLACK & WHITE FIGURE**

Figure 2. Kinetics of *in vitro* degradation. Hydrogels (100 µL) were incubated at 37°C in PBS. The percentage of weight loss was calculated at different time points. All the data are presented as mean±s.d. (n=4/group). **BLACK & WHITE FIGURE**

Figure 3. Evaluation of cytotoxicity for the four hydrogels. MTT assays were performed to determine the metabolic activity of L929 cells (a) cultured during 24 h in the presence of the media containing the leachables released by LMWHs during the first 24 hours (“24(1)”), and during the two following 24 hours “24(2)” and “24(3)”, respectively. As a positive control of toxicity, cells were also grown with the medium containing 0.1 % (v/v) Triton-X100 (“Toxic control”). The viability of L929 cells (b) was tested using neutral red assays with the same media. Results are expressed as percentage of the value obtained with the cells grown in the control medium. The dashed line shows the limit of toxicity (70%). All the data are presented as mean±s.d. (n=5/group). **BLACK & WHITE FIGURE**

Figure 4. Analysis of BSA adsorption on the four hydrogels. Hydrogels (100 μL with a surface area of 1.3 cm^2) were incubated for 2 hours at 37°C in 400 μL PBS containing either 2 mg/mL of bovine serum albumin (BSA) or not. After sodium dodecyl sulfate extraction, the proteins adsorbed to the hydrogels were quantified by BCA test. Statistical analysis with Kruskal-Wallis followed by Mann-Whitney tests (2-tailed) was performed to compare the adsorption of BSA to the four hydrogels (mean \pm s.d, $n=3$, $*p \leq 0.05$). **BLACK & WHITE FIGURE**

Figure 5. Masson's trichrome staining of hydrogels, and surrounding tissues dissected after 7 (a–d), and 21 d (e–h). Representative images showing the degradation and cell infiltration ($n=6/\text{group}$). * in the image denotes the position of the hydrogel. The images of Masson's trichrome staining after 7 d and 21 d after hydrogel injection are shown with magnified images at the lower panel. Blue staining indicates collagen and purple represents nuclei. The hydrogels are also stained in blue. Scale bars of $500\mu\text{m}$ for the upper panels and the magnified images are represented in lower panels with a scale bar $100\mu\text{m}$. Additional images are available in **Suppl Fig S5. COLOR FIGURE.**

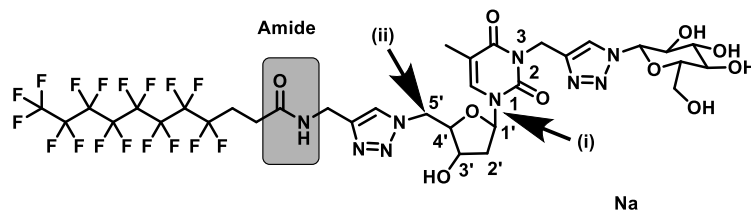
Figure 6. Foreign body response and angiogenesis. 21 d after implantation, the tissue was paraffin embedded and sections were stained with different antibodies; the hydrogels are shown by an asterisk (*) and their limit by a dashed line. **a)** Macrophage staining: CD68 (pan-macrophage marker, upper lane), the pro-inflammatory marker CCR7 (medium lane) and the immuno-modulatory marker CD206 (lower lane). M1 macrophages were found more inside the hydrogel, very few around the hydrogel and M2 were observed in the periphery of the hydrogels. **b)** Analysis of fibrosis: vimentin and α -SMA were detected as markers of fibroblasts and myofibroblasts, respectively. Vimentin-positive cells were visible in the tissue, but not at the interface with hydrogels. α -SMA was observed only to the smooth muscle cells of vessels around endothelial cells and Desmin was co-labeled with α -SMA to confirm staining of endothelial cells. Scale bar is $25\mu\text{m}$ ($n=4$ in each group). **c)** Angiogenesis at hydrogel/tissue interface: CD31 staining showed blood vessels in the tissue surrounding the hydrogels; arrows indicate some CD31 positive cells. Scale bar of 1 mm for upper panel and $100\mu\text{m}$ for magnified images at lower panel. **d)** Quantitative analysis of blood vessels counted in the vicinity of the four hydrogels (at least five different fields were randomly examined in each section). Statistical

significance was determined by Kruskal-Wallis and Mann Whitney (2-tailed analysis). All the data are presented as mean±s.d. (n=5/group), ** $p \leq 0.01$. **COLOR FIGURE.**

Figure 7. Angiogenesis analyzed in HUVECs and CAM assay. **a)** Chemical structure of the degradation by-product: the common peak observed in the mass spectra after hydrolysis of GNF, GNBA-1, and GNBA-3 was in the close agreement with the possible degradation by-product. Mimic of the possible by-product was synthesized chemically (called GN-1) (**Suppl. Fig. S1**). **b)** Cytotoxicity of the compound on HUVECs: different concentrations 2, 10, 20, 50, 100, 500, and 1000 μ M did not show any toxicity compared to the control (basal medium) (n=5). **c)** Migration study by scratch test on HUVECs: representative pictures of scratch assays at time lapse of 17h in basal medium EGM2 (Upper), basal medium + active compound: 1000 μ M (middle) and positive medium EGM2-MV. **d)** Percentage of filling during all the time lapse and speed of filling for each condition. **e)** Angiogenesis analyzed with CAM assay: representative photographs of the CAM on day 17, treated with vehicle (DMEM media alone, n=23), or 10 μ g of GN-1 (n=19). Photos of large fields of view (A, D, G) and magnified images before (B, E, H), and after (C, F, I) fixation with 4% PFA were done; the first column (A, B, C) shows a CAM with a normal (non-stimulated) angiogenesis; examples of CAMs exhibiting efficient sprouting (D, E, F), and tortuous capillaries (G, H, I) are shown. **f)** Quantification of the presence or absence of sprouting and tortuous vessels in the control and treated groups by blind screening (made independently by 5 observers), and the statistics performed by Fisher's exact test. **COLOR FIGURE.**

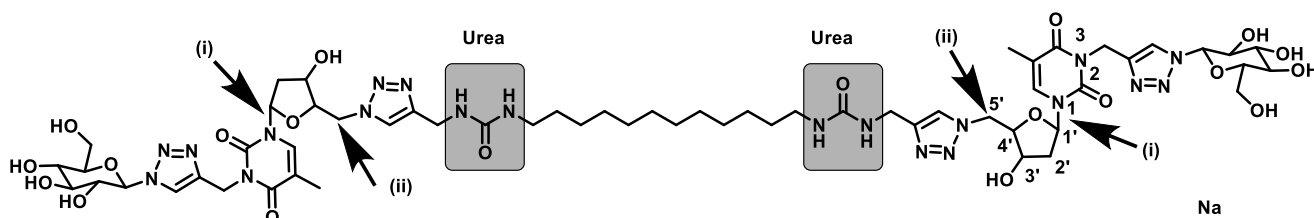
Figure 1.

GNF



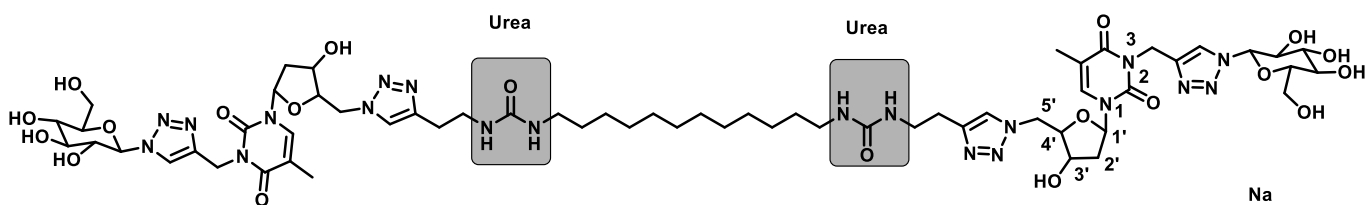
Chemical Formula: C₃₃H₃₄F₁₇N₉NaO₁₀
Molecular Weight: 1062.6506

GNBA-1



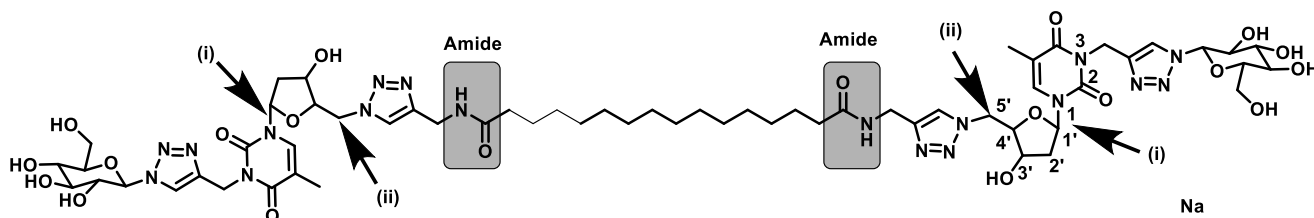
Chemical Formula: C₅₈H₈₆N₂₀NaO₂₀
Molecular Weight: 1406.4358

GNBA-2



Chemical Formula: C₆₀H₉₀N₂₀NaO₂₀
Molecular Weight: 1434.4898

GNBA-3



Chemical Formula: C₆₀H₈₈N₁₈NaO₂₀
Molecular Weight: 1404.4598

Figure 2.

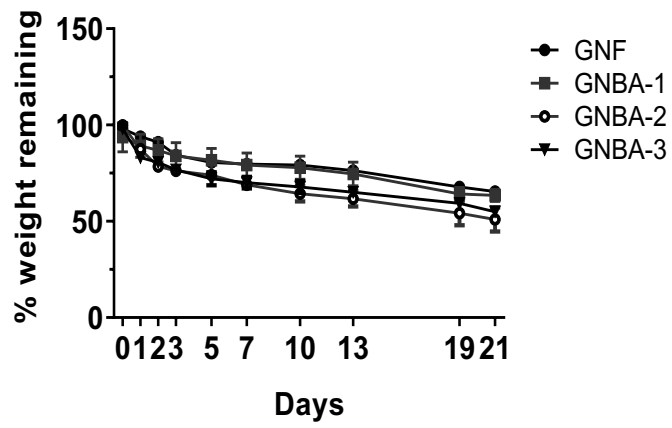
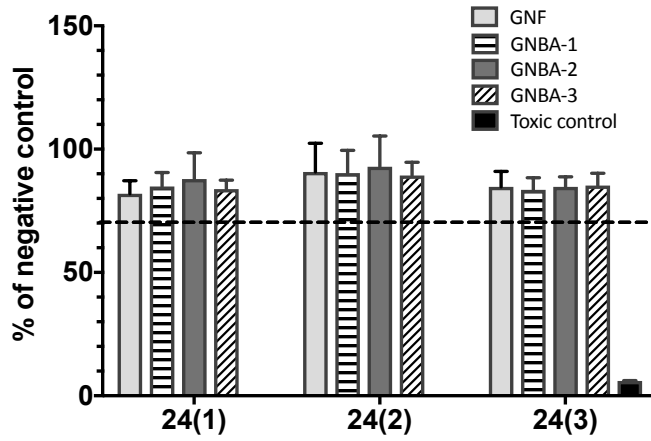


Figure 3.

(a) MTT assay on L929 (extracts)



(b) Neutral red assay on L929 (extracts)

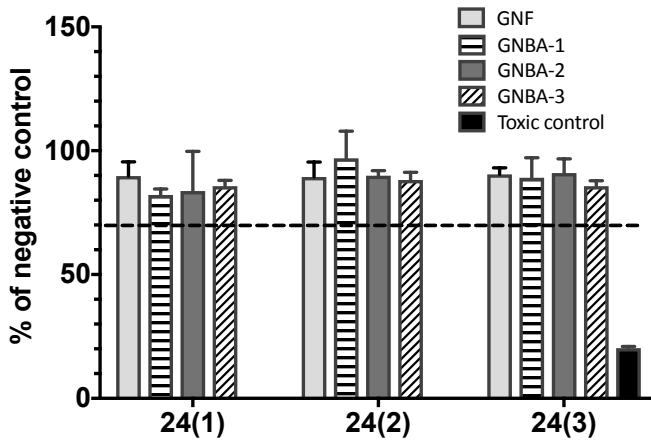


Figure 4.

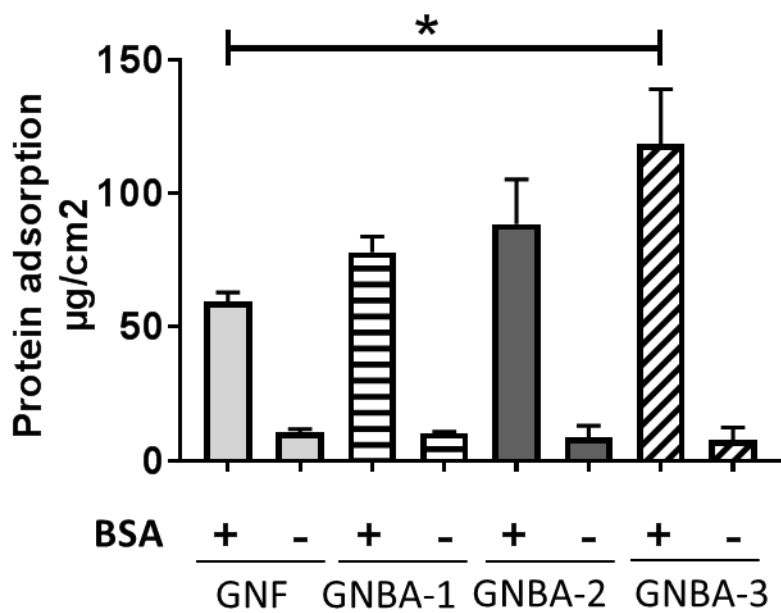


Figure 5.

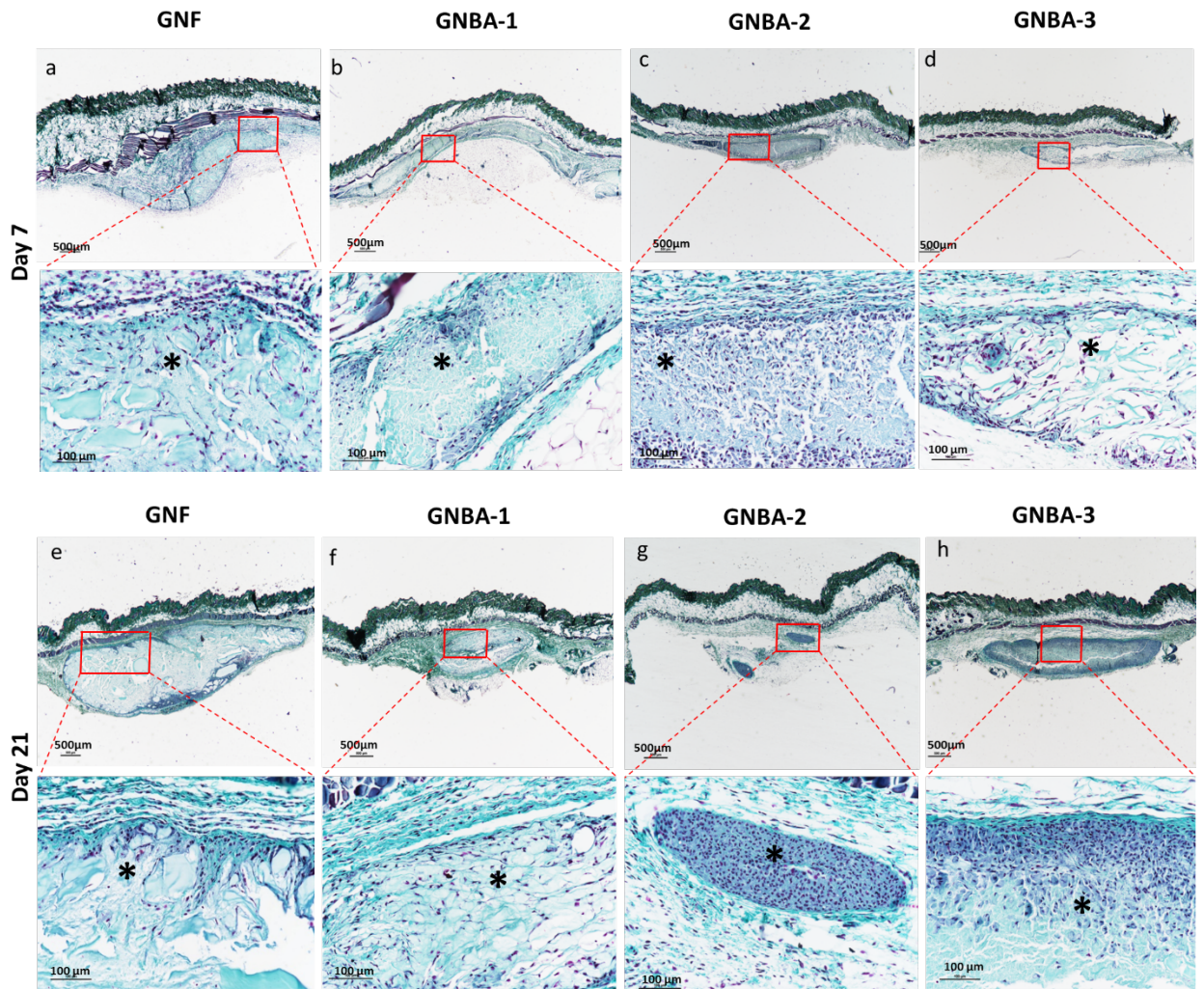


Figure 6a, b.

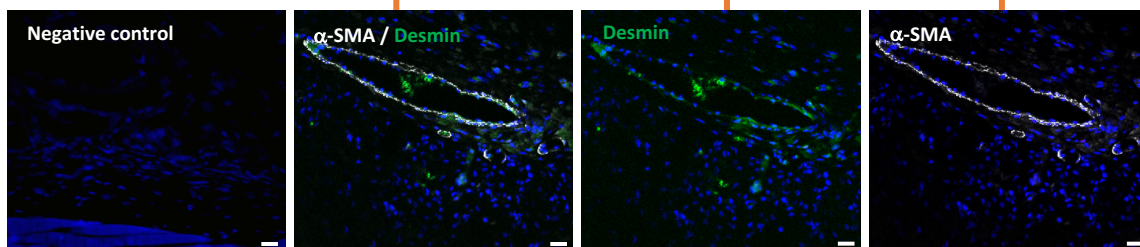
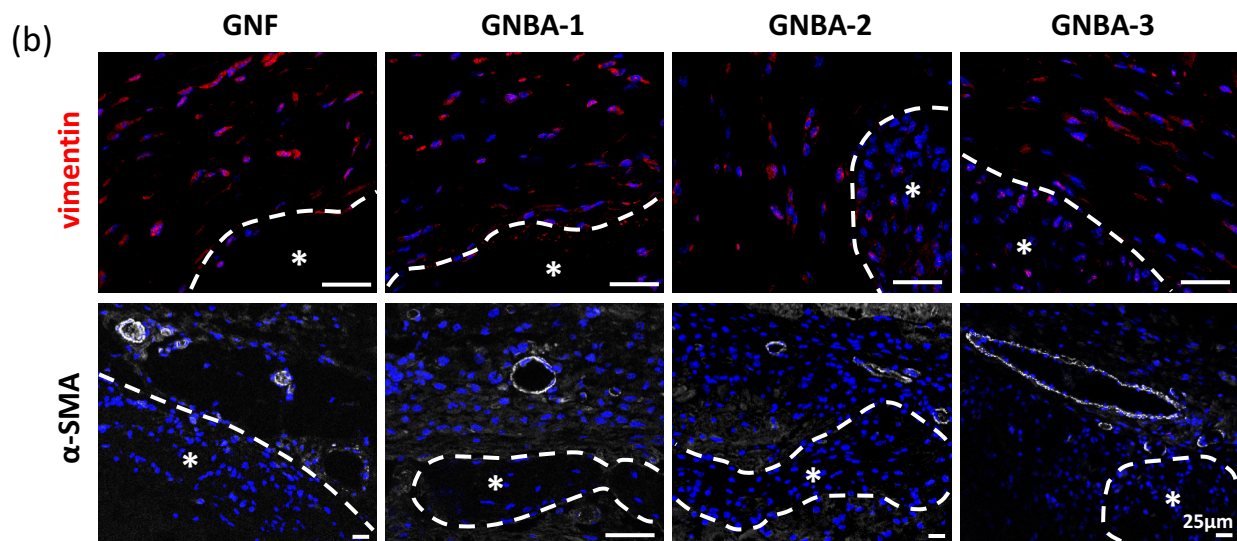
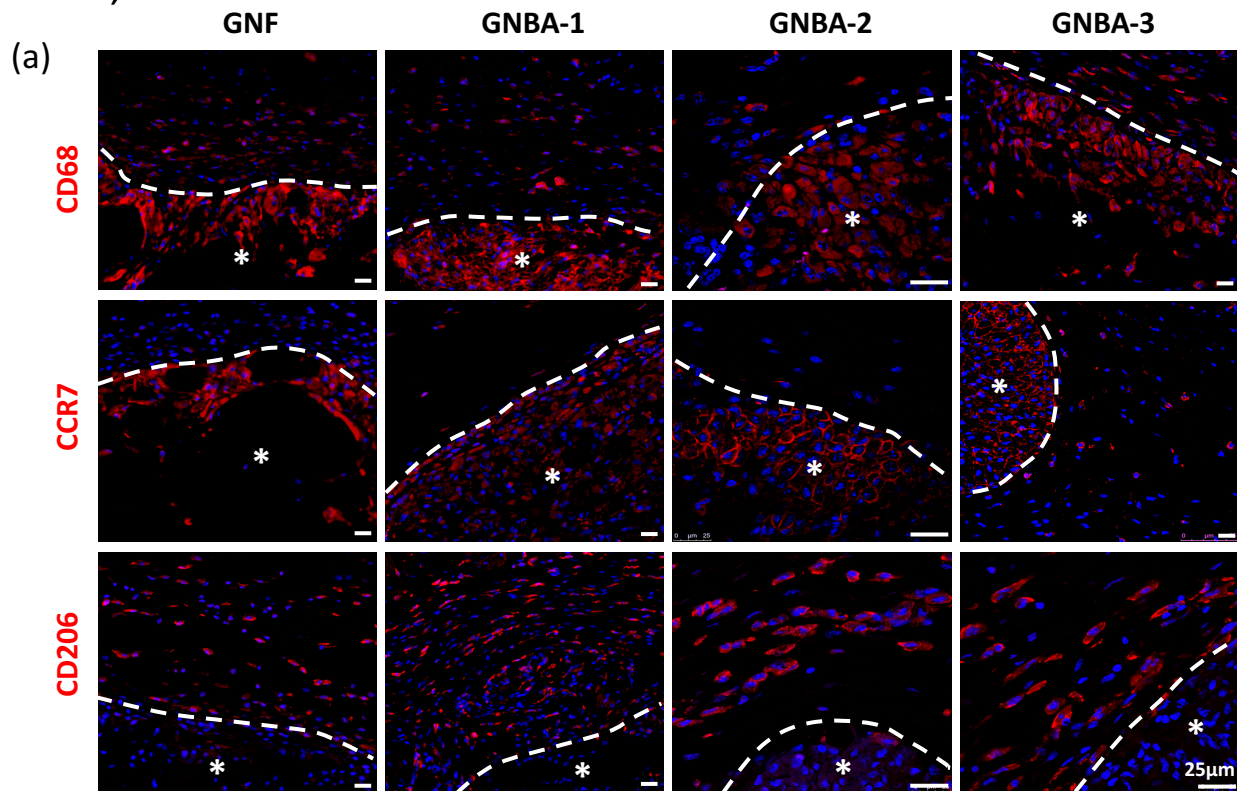


Figure 6c, d.

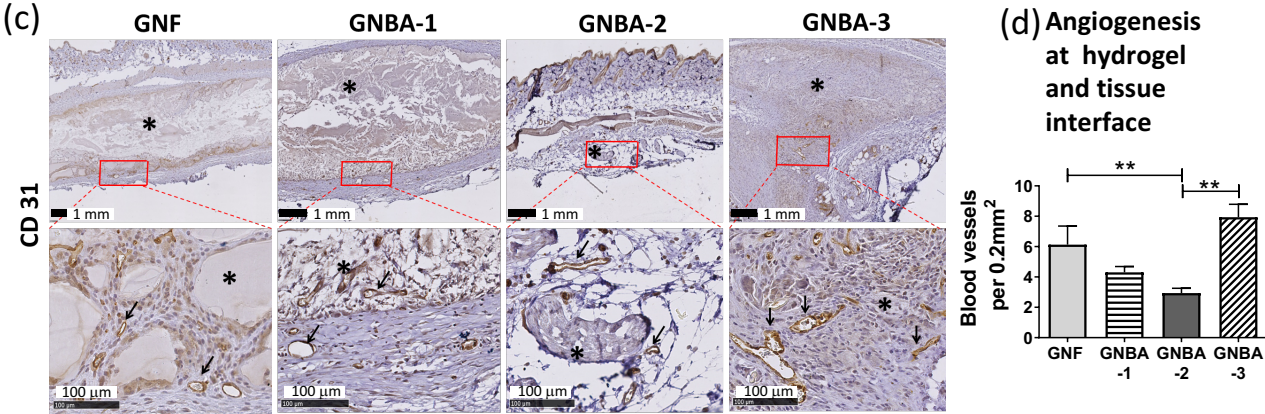
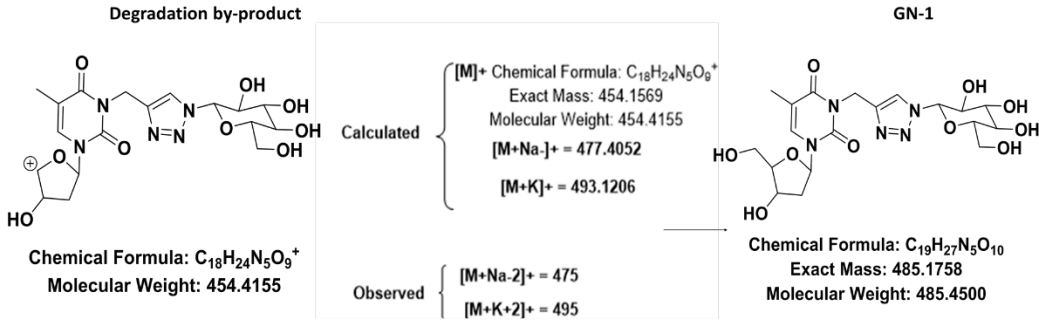
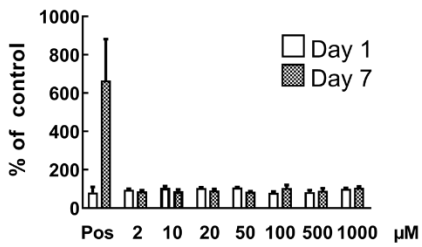


Figure 7.

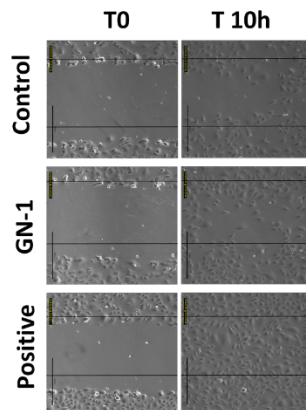
(a) Chemical structure of degradation by-product and of GN-1



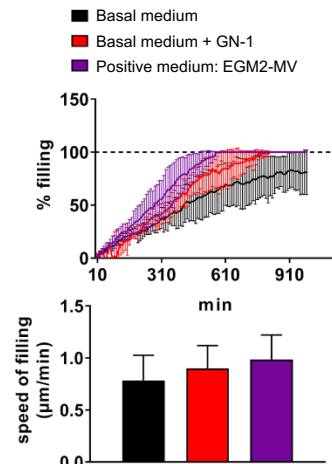
(b) Cytotoxicity of GN-1 on HUVEC Cells



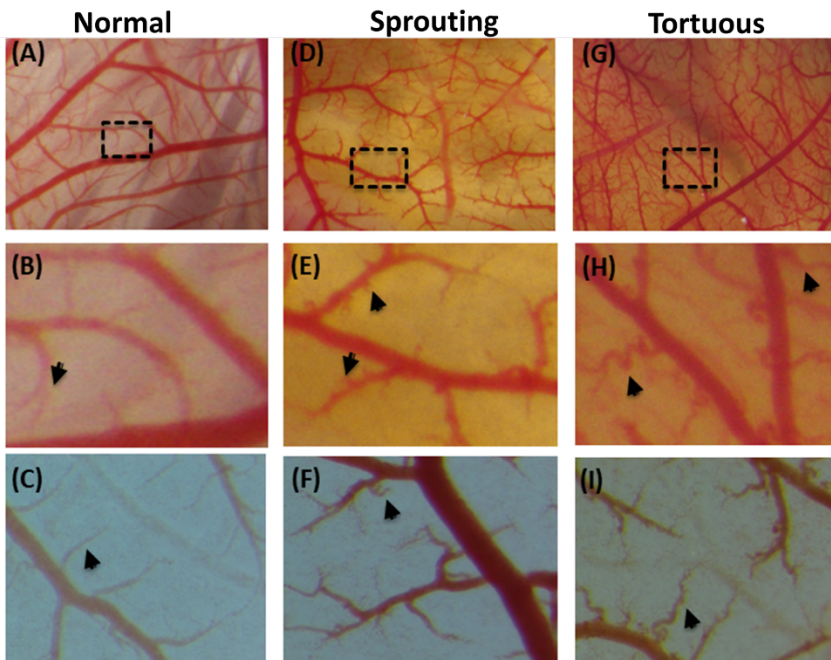
(c) Migration study by scratch test



(d) Quantification of migration study



(e) Angiogenesis analysed by CAM assay.



(f) Quantification of the presence or absence of sprouting and tortuous vessels

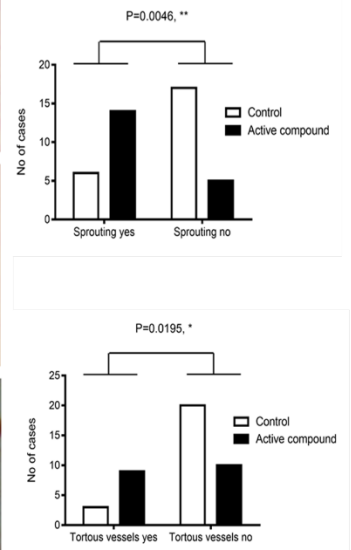
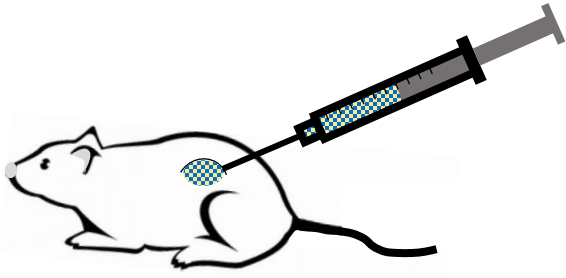








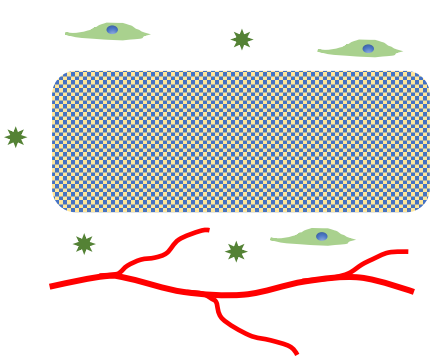


Table 1

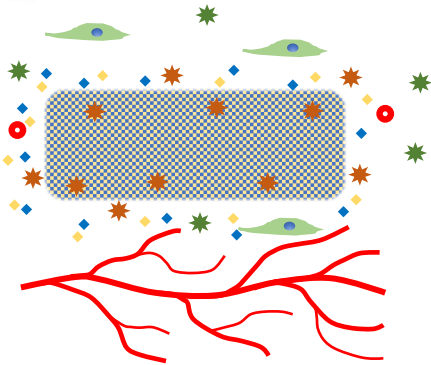
LMWHs	Fragments	Cleavage	Mass calculated	Mass observed
GNF	First fragmentation (I)	C1'-N1	Fragment 1: 734.41 [M+Na+K] ⁺ Fragment 2: 369.33 [M+Na] ⁺	731.12 [M+Na+K] ⁺ (Peak 2) 368.00 [M] ⁺ (Peak 4)
	Second fragmentation (II)	CH2-Methylene CH2	Fragment 3: 492.42 [M] ⁺	495.04 [M+Na] ⁺ (Peak 3)
GNBA-1	First fragmentation (I)	C1'-N1 Methylene	Fragment 2: 733.68 [M+2Na+K] ⁺	731.17 [M+2Na+K] ⁺ (Peak 2)
	Second fragmentation (II)	C4 Methylene CH ₂	Fragment 4: 476.33 [M] ⁺ Fragment 1: 969.13 [M+K] ⁺	475.47 [M] ⁺ (Peak 3) 967.21 [M+K] ⁺ (Peak 4)
GNBA-2	No fragmentation observed			
GNBA-3	First fragmentation (I)	C1'-N1 Methylene	Fragment 1: 736.40 [M+Na+K] ⁺	731.13 [M+Na+K] ⁺ (Peak 2)
	Second fragmentation (II)	C4 Methylene CH ₂	Fragment 3: 474.65 [M] ⁺ Fragment 2: 990.15 [M+Na+K] ⁺	473.06 [M] ⁺ (Peak 3) 989.16 [M+Na+K] ⁺ (Peak 4)



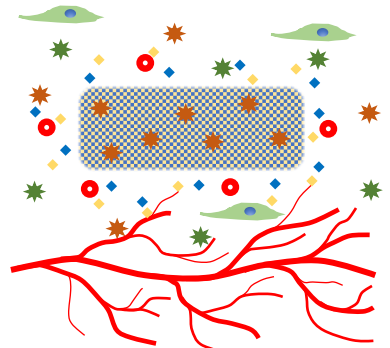
Host cells		Hydrogel's compounds	
	Fibroblasts		Hydrogel
	M1 macrophages		Intact molecule
	M2 macrophages		Degraded molecule
	Blood vessels		Angiogenic compound



Day 0



Day 7



Day 21